Computer Methods and Recent Advances in Geomechanics – Oka, Murakami, Uzuoka & Kimoto (Eds.)
© 2015 Taylor & Francis Group, London, ISBN 978-1-138-00148-0

Instability analysis and numerical simulation of the dissociation process of methane hydrate bearing soil

H. Iwai, S. Kimoto, T. Akaki & F. Oka
Department of Civil and Earth Resources Engineering, Kyoto University, Kyoto, Japan

ABSTRACT: Methane hydrates have been viewed as a new potential energy source, since a large amount of methane gas is trapped inside the hydrates. It is, however, well known that dissociation process of methane hydrate may lead to unstable behavior such as large deformation, uncontrollable gas production etc. A linear instability analysis was performed in order to investigate which variables have a significant effect on the onset of the instability of methane hydrate bearing soils with a simplified viscoplastic constitutive equation subjected to dissociation. Then, we conducted a numerical analysis of gas hydrate bearing soil with dissociation in order to investigate the effect of the rate of hydrate dissociation on the system. From the numerical results, the larger pore gas pressure and pore water pressure are produced and they diverge when the methane hydrate dissociation rate is relatively higher.

1 INTRODUCTION

Recently, methane hydrates have been viewed as a potential energy resource since a large amount of methane gas is trapped inside the hydrates. A unit volume of methane hydrate dissociates into approximately 160–170 times of volume of methane gas. We do not have, however, enough knowledge about behaviors of methane hydrates bearing sediments induced by dissociation. Some researchers have pointed out that gas hydrates may be a trigger of submarine geohazard (e.g., Sultan et al. 2004a, b). Wu et al. (2008) showed the possibility that the dissociation of methane hydrates causes significant increase in the pore pressure and thus significant decrease in the effective stress under undrained conditions through the laboratory tests. In addition, many experimental studies indicate that the loss of bonding effects of hydrates between soil particles in sediments may lead to the decrease in the stiffness and the strength (e.g., Hyodo et al. 2014, Waite et al. 2009). Recently, several numerical models that can simulate the flow and deformation behavior during hydrate dissociation have been developed by many researchers and institutions. Kimoto et al. (2010) have developed a numerical simulator for deformation of soil containing methane hydrates in order to predict ground stability during hydrate dissociation, in which an elasto-viscoplastic model considering the effect of suction and the hydrate saturation is used for soil sediments. From the numerical results, they reported that ground deformation is induced by generation and dissipation of the water pressure and the gas pressure, and it localizes around the hydrate dissociation area.

Many experimental and numerical studies have been conducted on the deformation behavior associated with methane hydrate dissociation. Nevertheless, few theoretical studies to investigate the onset of instability subjected to hydrate dissociation such as linear stability analysis have been performed. The instability analysis for a water saturated soil has been widely studied by many researchers. Rice (1975) investigated a stability of fluid saturated porous material in quasi-static conditions. Anand et al. (1987) and Zibib & Aifantis (1988) conducted linear perturbation stability analysis for the onset of shear localization. Oka et al. (1995) have been dealing with the strain localization problem of water saturated clay through the use of viscoplastic constitutive equations because of the rate dependent nature of cohesive soil. Higo et al. (2005) have studied the effect of permeability and initial heterogeneity on the strain localization of water saturated soil. Garcia et al. (2010) have performed a linear stability analysis in order to investigate which variables have a significant effect on the onset of the instability of an unsaturated viscoplastic material subjected to water infiltration. They have found that the onset of growing instability of the material system mainly depends on the specific moisture capacity, the suction and the hardening parameter.

In the present study, we have conducted a linear stability analysis to investigate the onset of instability during dissociation process. Figure 1 shows an illustration of the stable and unstable regions of methane hydrate bearing sediments with and without hydrates dissociation. We discuss which parameters or variables have a significant effect on the instability of methane

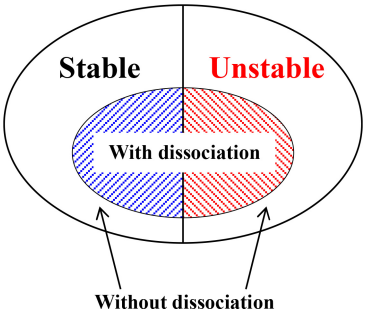

Figure 1. Illustrative view of the stable and unstable regions of methane hydrate bearing sediments with and without dissociation.

hydrates bearing materials when they are subjected to a dissociation process.

2 INSTABILITY ANALYSIS OF METHANE HYDRATE BEARING VISCOPLASTIC MATERIAL

In this section, the linear stability analysis of methane hydrate bearing soil considering dissociation is shown. We followed basically the method by Garcia et al. (2010), and extended the method by considering energy balance and hydrates reaction process in order to deal with the dissociation phenomenon. The governing equations for the chemo-thermo-mechanically coupled behavior are based on Kimoto et al. (2010), and a viscoplastic constitutive model for the soil skeleton is used. The details of the one-dimensional governing equations for the stability analysis are shown in the following.

2.1 *Stress variables*

When modeling the mechanical behavior of an unsaturated soil, it is necessary to choose appropriate stress variables since they control its mechanical behavior. In this study, we use the skeleton stress for the stress variable for the soil skeleton (Oka et al. 2008). The total stress σ is obtained from the sum of the partial stresses for each phase,

$$\sigma = \sigma^S + \sigma^H + \sigma^W + \sigma^G \tag{1}$$

where superscripts S, H, W, G indicate soil, hydrate, water and gas phase, respectively. The partial stresses for the fluid phases can be written as

$$\sigma^W = -n^W P^W \tag{2}$$

$$\sigma^G = -n^G P^G \tag{3}$$

where P^W, P^G, n^W and n^G are the pore water pressure, the pore gas pressure, the volume fraction of the water phase and the volume fraction of the gas phase, respectively. Tension is positive for the stresses. For simplicity, we assume that soil phase and hydrate phase are in the same phase, namely, solid phase. Thus the partial stress of solid phase is defined as:

$$\sigma^{SH} = \sigma^S + \sigma^H \tag{4}$$

$$\sigma^{SH} = \sigma' - n^{SH} P^F \tag{5}$$

$$n^{SH} = n^S + n^H \tag{6}$$

where σ' is called skeleton stress in the present study. The terms n^S and n^H are volume fraction of the soil phase and the hydrate phase, respectively, and P^F is the average fluid pressure given by

$$P^F = sP^W + (1-s)P^G \tag{7}$$

where s is the water saturation. Substituting Eqs. (2)∼(7) into Eq. (1), the skeleton stress is obtained as

$$\sigma' = \sigma + P^F \tag{8}$$

2.2 *Mass conservation law*

The mass conservation law for four phases is given by

$$\frac{D^\alpha}{Dt}\left(n^\alpha \rho^\alpha\right) + n^\alpha \rho^\alpha \frac{\partial v^\alpha}{\partial x} - \dot{m}^\alpha = 0 \tag{9}$$

where ρ^α is the material density for α phase, v^α is the velocity vector of each phase, and $\dot{m}^\alpha$ is the mass increasing rate per unit volume due to hydrate dissociation. We use three assumptions. The first is that the densities of the soil, the water and the hydrate are constant, that is, $\dot{\rho}^S = \dot{\rho}^W = \dot{\rho}^H = 0$, where superimposed dot denotes the material time derivative, and the density of the gas phase follows the equation for ideal gas. Second, the soil particles and hydrates move together, namely,

$$v^S = v^H = v^{SH} \tag{10}$$

Third one is that the spatial gradient of velocity of solid phase is equal to the strain rate.

$$\frac{\partial v^S}{\partial x} = \frac{\partial v^H}{\partial x} = \frac{\partial v^{SH}}{\partial x} = \dot{\varepsilon} \tag{11}$$

Considering these assumptions and Eq. (9), we obtain the continuity equations for the water and gas phases.

$$s\dot{\varepsilon} + \dot{s}n^F + \frac{\partial V^W}{\partial x} + \left(s\frac{\dot{m}^H}{\rho^H} - \frac{\dot{m}^W}{\rho^W}\right) = 0 \tag{12}$$

$$(1-s)\dot{\varepsilon} - \dot{s}n^F + \frac{\partial V^G}{\partial x} + (1-s)n^F\left(\frac{\dot{P}^G}{P^G} - \frac{\dot{\theta}}{\theta}\right) + \left\{(1-s)\frac{\dot{m}^H}{\rho^H} - \frac{\dot{m}^G}{\rho^G}\right\} = 0 \tag{13}$$

where n^F is the volume fraction of the fluid phase and V^W, V^G are the relative velocities defined as:

$$V^\beta = n^\beta\left(v^\beta - v^{SH}\right), \quad (\beta = W, G) \tag{14}$$

2.3 *Darcy type's law*

Darcy type's law for the flows of the water and the gas can be described as follows:

$$V^W = -\frac{k^W}{\gamma^W}\left(\frac{\partial P^W}{\partial x} - \rho^W \overline{F}\right), \quad \gamma^W = \rho^W g \tag{15}$$

$$V^G = -\frac{k^G}{\gamma^G}\left(\frac{\partial P^G}{\partial x} - \rho^G \overline{F}\right), \quad \gamma^G = \rho^G g \tag{16}$$

where $\overline{F}$ is the body force such as gravitational force per unit mass, k^W and k^G are the permeability coefficients for the water and the gas phases, respectively, and g is gravitational acceleration.

2.4 *Equilibrium equation*

The one-dimensional equilibrium equation can be written as:

$$\frac{\partial \sigma}{\partial x} + \rho \overline{F} = \frac{\partial \sigma'}{\partial x} - \frac{\partial P^F}{\partial x} + \rho \overline{F} = 0 \tag{17}$$

2.5 *Energy conservation law*

In the present study, we consider heat conductivity and heat change rate $\dot{Q}^H$ associated with the hydrate dissociation. The one-dimensional equation of energy conservation is written as:

$$\dot{\theta} = \frac{1}{\rho c}\left(k^\theta \frac{\partial^2 \theta}{\partial x^2} + \dot{Q}^H\right) \tag{18}$$

$$\rho c = \sum_\alpha n^\alpha \rho^\alpha c^\alpha \quad , k^\theta = \sum_\alpha n^\alpha k^\alpha \tag{19}$$

$$\dot{Q}^H = (a - b\theta)\frac{\dot{N}_H}{V}, \ a = 56599, \ b = 16.744 \tag{20}$$

Where c^α and k^α are the specific heat and the heat conductivity of phase α, respectively, and θ is temperature for all phases, and $\dot{Q}^H$ is time rate of dissociation heat per unit volume due to the hydrate dissociation.

2.6 *Dissociation rate of methane hydrate*

Methane hydrate dissociates into water and gas with the reaction expressed in Eq. (21).

$$CH_4 \cdot 5.75H_2O\,(\text{hydrate}) \rightarrow CH_4(\text{gas}) + 5.75H_2O\,(\text{liquid}) \tag{21}$$

We use Kim-Bishnoi's equation for the methane hydrate dissociation rate $\dot{N}_H$ (Kim et al. 1987).

$$\dot{N}_H = -D_H \exp\left(-\frac{9400}{\theta}\right)\left(P^e - P^F\right) N_{H0}^{\frac{1}{3}} N_H^{\frac{2}{3}} \tag{22}$$

where N_H is the moles of hydrates in the volume V, N_{H0} is the moles of hydrates in the initial state, P^e is an equilibrium pressure at the temperature θ, and D_H is the coefficient of hydrate dissociation rate.

2.7 *Viscoplastic constitutive equation*

In the numerical simulations, we use the viscoplastic constitutive equations taking into account the dependency on the hydrate saturation and the suction (Kimoto et al. 2010), however in the stability analysis, a simplified viscoplastic constitutive model is used for simplicity. The stress-strain relation can be expressed as

$$\sigma' = H\varepsilon + \mu\dot{\varepsilon} \tag{23}$$

where ε is the strain, $\dot{\varepsilon}$ is the strain rate, H is the strain hardening-softening parameter and μ is the viscoplastic parameter. We assume that the strain hardening-softening parameter H is a function of the suction P^C and the hydrate saturation S_r^H for simplicity. The viscoplastic parameter μ is a function of the temperature θ, namely,

$$H = H\left(P^C, S_r^H\right), \quad \mu = \mu(\theta) \tag{24}$$

$$P^C = P^G - P^W \tag{25}$$

$$S_r^H = \frac{V^H}{V^v} = \frac{n^H}{n} \tag{26}$$

2.8 *Perturbed governing equation*

In order to estimate the instability of the material system, we consider the governing equations described above in a perturbed configuration. In those equations, the unknowns are the pore water pressure P^W, the pore gas pressure P^G, the strain ε, the temperature θ, and the moles of hydrate N_H. For each unknown, we suppose that

$$\begin{aligned} &P^W = P_{(0)}^W + \tilde{P}^W, \ P^G = P_{(0)}^G + \tilde{P}^G, \ \varepsilon = \varepsilon_{(0)} + \tilde{\varepsilon} \\ &\theta = \theta_{(0)} + \tilde{\theta}, \ N_H = N_{H(0)} + \tilde{N}_H \end{aligned} \tag{27}$$

where the first terms in right side in Equation (27) indicate the values which satisfy the governing equations and second terms are the perturbations of each variables. For the perturbations, we assume the periodic form as follows:

$$\left[\tilde{P}^W, \tilde{P}^G, \tilde{\varepsilon}, \tilde{\theta}, \tilde{N}_H\right]^T = \left[P^{W*}, P^{G*}, \varepsilon^*, \theta^*, N_H^*\right]^T \exp(\omega t + iqx) \tag{28}$$

where q is the wave number, ω is the rate of the fluctuation growth, and superscript ( )* indicates the amplitude of each variable. Substituting Eq. (27) into Eqs. (12), (13), (17), (18), (22), and considering Eq. (28), the perturbed governing equations can be rewritten in matrix form.

$$[\mathbf{A}]\{\mathbf{y}\} = \{\mathbf{0}\}, \quad \{\mathbf{y}\} = \left\{P^{W*}, P^{G*}, \varepsilon^*, \theta^*, N_H^*\right\}^T \tag{29}$$

From the non-zero conditions for the amplitudes, we obtain a following polynomial equation.

$$a_5\omega^5 + a_4\omega^4 + a_3\omega^3 + a_2\omega^2 + a_1\omega + a_0 = 0 \tag{30}$$

When the growth rate of the perturbations ω has a positive real part, the fluctuations grow as time progresses, namely the system becomes unstable. On the contrary, if the real part of ω is negative, the material system is stable. The necessary and sufficient conditions that the all roots have negative real parts are given by the Routh-Hurwitz criteria.

Considering the criteria, if at least one coefficient of Eq. (30) has different sign from others, it is possible that the real part of ω becomes positive, and the material system can be unstable. We discuss the sign of the coefficient a_5 and a_0.

$$a_5 = -B_C n^F \mu \frac{(1-s)n^F}{P^G} \tag{31}$$

$$a_0 = \frac{C_N}{\rho c}\left(H - \varepsilon H_{SH}\frac{n^H}{n^2}\right)\frac{k^W}{\gamma^W}\frac{k^G}{\gamma^G}q^4\left(k^\theta q^2 + \dot{N}_H b\right) \tag{32}$$

where H_{SH} is the partial derivative of H with respect to the hydrate saturation S_r^H, namely,

$$H_{SH} = \frac{\partial H}{\partial S_r^H} \tag{33}$$

and C_N is the partial derivative of $\dot{N}_H$ with respect to the moles of hydrates N_H, namely,

$$C_N = -\frac{\partial \dot{N}_H}{\partial N_H} = \frac{2}{3}D_H \exp\left(-\frac{9400}{\theta}\right)\left(P^e - P^F\right)\left(N_{H0}/N_H\right)^{\frac{1}{3}} \tag{34}$$

Note that the sign of $q, s, n, n^F, n^H, H_{SH}, k^W, k^G, k^\theta, \gamma^W, \gamma^G, \rho c, C_N, b, P^G$ are always positive, whereas the sign of B_C and $\dot{N}_H$ is always negative. The sign of the strain ε is positive in expansion and is negative in compression, and the strain rate $\dot{\varepsilon}$ can be positive or negative. The strain softening-hardening parameter H is positive in viscoplastic hardening and is negative in viscoplastic softening. Considering that the sign of each term and Eq. (31), the sign of a_5 is always positive, whereas there is a possibility that the sign of a_0 becomes negative in the following two cases.

$$k^\theta q^2 + \dot{N}_H b < 0 \quad \text{and} \quad H - \varepsilon H_{SH}\frac{n^H}{n^2} > 0 \tag{35}$$

$$k^\theta q^2 + \dot{N}_H b > 0 \quad \text{and} \quad H - \varepsilon H_{SH}\frac{n^H}{n^2} < 0 \tag{36}$$

The term of $k^\theta q^2 + \dot{N}_H b$ is negative when the magnitude of hydrate dissociation rate $|\dot{N}_H|$ is larger than $k^\theta q^2/b$, where the instability conditions are given by Eq. (35). The condition $H - \varepsilon H_{SH} n^H/n^2 > 0$ is satisfied in the case of viscoplastic hardening $H > 0$ with the compressive strain $\varepsilon < 0$, or with the expansive strain which satisfies the following inequality.

$$0 < \varepsilon H_{SH}\frac{n^H}{n^2} < H \tag{37}$$

In contrast, the term of $k^\theta q^2 + \dot{N}_H b$ is positive when the hydrate dissociation rate $|\dot{N}_H|$ is smaller than $k^\theta q^2/b$. In this case, the instability conditions are given in Eq. (36). The condition $H - \varepsilon H_{SH} n^H/n^2 < 0$ is satisfied in the case of the viscoplastic softening $H < 0$ with the expansive strain $\varepsilon > 0$, or with the compressive strain $\varepsilon < 0$ which satisfies the following inequality.

$$H < \varepsilon H_{SH}\frac{n^H}{n^2} < 0 \tag{38}$$

3 NUMERICAL ANALYSIS BY THE MULTI PHASE COUPLED MODEL

We conducted a numerical analysis of gas hydrate bearing soil with dissociation in order to investigate the effect of the rate of hydrate dissociation on the system.

3.1 *Initial and boundary conditions*

Figure 2 shows the model of seabed ground and the finite element mesh used in the analysis with boundary conditions. The seabed ground from the bottom of the seabed to 400 m in depth is modeled under two-dimensional plane strain conditions. The seabed is at a depth of 1000 m. The methane hydrate-bearing layer exists at a ground depth of 264–328 m. We assume the depressurization method for hydrate dissociation, and the depressurizing source exists in the center of hydrate layer with length of 32 m.

We apply the hydrostatic pressure at the top, bottom, and right boundaries. The left boundary is set to be adiabatic boundary and impermeable for water and

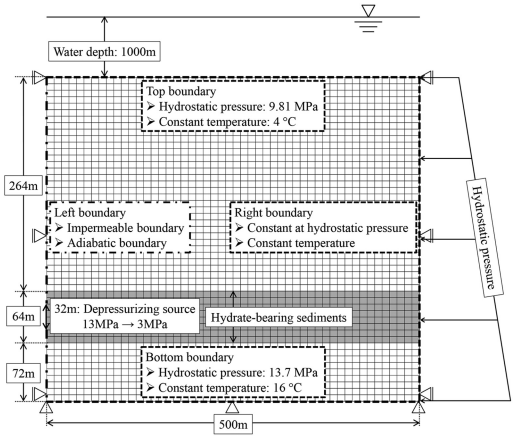

Figure 2. Finite element mesh and boundary conditions.

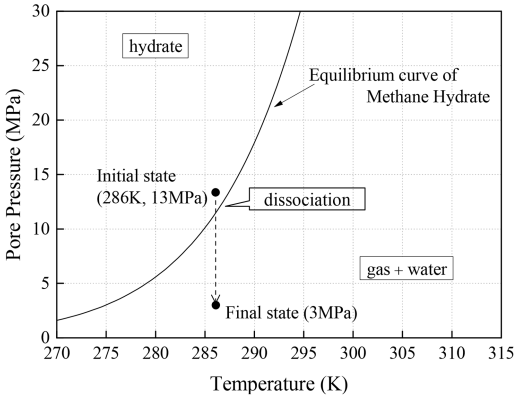

Figure 3. Equilibrium curve of methane hydrate, initial and final conditions of simulation.

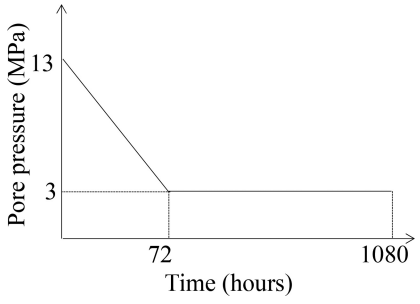

Figure 4. Pore pressure-time profile at the boundary.

gas except for depressurizing source for the symmetric boundary conditions. The initial and final states of pressure and temperature at the source are shown in Figures 3 and 4. The initial pore gas pressure is the same as the pore water pressure. The pore pressures around the source are about 13 MPa, and they are linearly reduced to 3 MPa in 72 hours. The initial and material parameters are listed in Table 1.

3.2 *Simulation cases*

In order to investigate the effects of the hydrate dissociation rate $\dot{N}_H$, we have analyzed three cases with different values of D_H in Eq. (21) as listed in Table 2.

3.3 *Simulation results*

In Case1, the pore gas pressure increased drastically at 12.7 hours due to the hydrate dissociation, and then it dissipated with the depressurization progresses. On the other hand, in the case of large dissociation rate, the pore gas pressure diverged unstably at 14.7 hours in Case2 and 12.7 hours in Case3 as shown in Figure 5. Figure 6 indicates time profiles of the pore water pressure in Element 111 and Element 113. The behavior of the pore water pressure is similar to the excess pore gas pressure. In Case2 and Case3 the pore water pressure diverged both in Element 111 and Element 113.

Table 1. Material parameters for methane hydrate-bearing sediments.

Initial void ratio	e_0	0.89
Initial water saturation	s_{r0}	1.0
Initial hydrate saturation	S_{r0}^H	0.51
Compression index	λ	0.169
Swelling index	κ	0.017
Initial shear elastic modulus	G_0	53800 (kPa)
Viscoplastic parameter	C_0	1.0×10^{-12} (1/s)
Viscoplastic parameter	m'	23.0
Stress ratio at critical state	M_f^*	1.09
Parameter for suction effect	P_i^C	100 (kPa)
Parameter for suction effect	S_I	0.2
Parameter for suction effect	s_d	0.25
Parameter for hydrate effect	S_{ri}^H	0.51
Parameter for hydrate effect	n_m	0.6
Parameter for hydrate effect	n_d	0.75
Thermo-viscoplastic parameter	α	0.15
Permeability for water	k^W	1.0×10^{-5} (m/s)
Permeability for gas	k^G	1.0×10^{-4} (m/s)

Table 2. Simulation cases.

Case No.	D_H (1/MPa · s)
Case 1	5.85×10^{12}
Case 2	5.85×10^{13}
Case 3	5.85×10^{14}

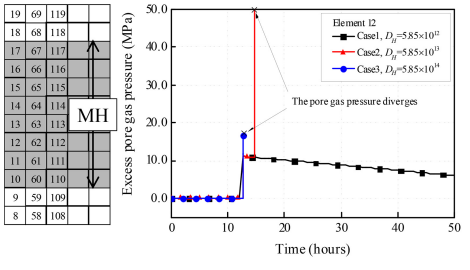

Figure 5. Time profiles of the excess pore gas pressure.

Figure 7 shows the distributions of the pore water pressure at the time when it reached the maximum value. The pore water pressure around the depressurization source decreased with depressurizing, whereas it increased around the area where the hydrate dissociates in every case. The pore water pressure reached 14379 kPa in Case1, 14400 in Case2, and 30874 kPa in Case3. The larger the hydrate dissociation rate is, the pore water pressure increases due to the dissociation. The rapid increase of pore gas pressure and water pressure affects the deformation behavior such as volumetric strain as shown in Figure 8. The compressive volumetric strain concentrated around the depressurization source for each case. The magnitude of compressive volumetric strain increased with an increase of the hydrate dissociation rate. These results are consistent with the results obtained from the linear stability analysis.

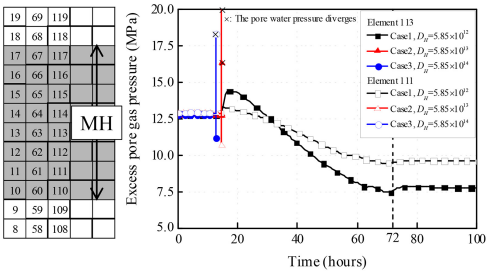

Figure 6. Time profiles of the pore water pressure.

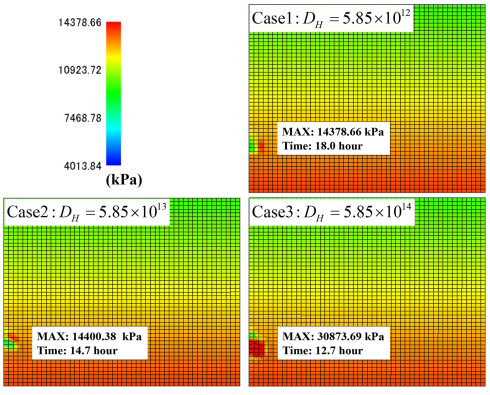

Figure 7. Distributions of the pore gas pressure.

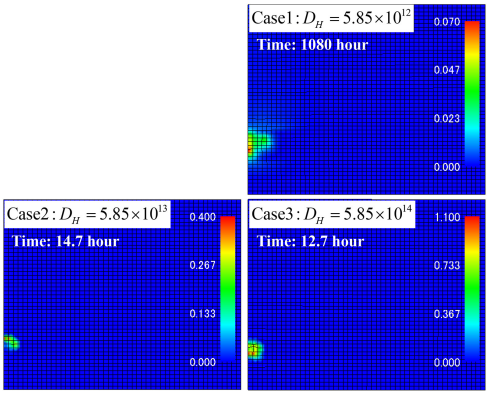

Figure 8. Distributions of the volumetric strain.

4 CONCLUSION

We performed a linear stability analysis in order to investigate the effects of the parameters on the onset of instability of hydrate bearing sediments. From the analysis, we found that the material system is possible to be unstable in the case with large value of the dissociation rate. In addition to the analysis, we conducted the numerical simulations, and the results are consistent with the results of the linear stability analysis.

ACKNOWLEDGEMENT

This work has been supported by JSPS KAKENHI Grant Number 24560604 and Grant-in-Aid for JSPS Fellows. We are grateful for their support.

REFERENCES

Anand, L. Kim, K.H. & Shawki, T.G. 1987. Onset of shear localization in viscoplastic solids. *Journal of the Mechanics and Physics of Solids* 35(4): 407–429.

Garcia, E. Oka, F. & Kimoto, S. 2010. Instability analysis and simulation of water infiltration into an unsaturated elasto-viscoplastic material. *International Journal of Solids and Structures* 47(25–26): 3519–3536.

Higo, Y. Oka, F. Jiang, M. & Fujita, Y. 2005. Effects of transport of pore water and material heterogeneity on strain localization of fluid-saturated gradient-dependent viscoplastic geomaterial. *International Journal for Numerical and Analytical Methods in Geomechanics* 29(April 2004): 495–523.

Hyodo, M. Li, Y. Yoneda, J. Nakata, Y. Yoshimoto, N. & Nishimura, A. 2014. Effects of dissociation on the shear strength and deformation behavior of methane hydrate-bearing sediments. *Marine and Petroleum Geology* 51: 52–62.

Kim, H.C. Bishnoi, P.R. Rizvi, S.S.H. & Engineering, P. 1987. Kinetics of methane hydrate decomposition. *Chemical Engineering Science* 42(1983): 1645–1653.

Kimoto, S. Oka, F. & Fushita, T. 2010. A chemo-thermo-mechanically coupled analysis of ground deformation induced by gas hydrate dissociation. *International Journal of Mechanical Sciences* 52(2): 365–376.

Oka, F. Adachi, T. & Yashima, A. 1995. A strain localization analysis using a viscoplastic softening model for clay. *International Journal of Plasticity* 11(5): 523–545.

Oka, F. Feng, H. Kimoto, S. Kodaka, T. & Suzuki, H. 2008. A numerical simulation of triaxial tests of unsaturated soil at constant water and air content by using an elasto-viscoplastic model, in: Toll, D.G., & Wheeler, S.J. (Eds.), Proceeding of the 1st European Conference on Unsaturated Soils. Taylor & Francis, pp. 735–741.

Rice, J.R. 1975. On the Stability of Dilatant Hardening for Saturated Rock Masses. *Journal of Geophysical Research* 80(11): 1531–1536.

Sultan, N. Cochonat, P. Canals, M. Cattaneo, A. Dennielou, B. Haflidason, H. Laberg, J.S. Long, D. Mienert, J. Trincardi, F. Urgeles, R. Vorren, T.O. & Wilson, C. 2004a. Triggering mechanisms of slope instability processes and sediment failures on continental margins: a geotechnical approach. *Marine Geology* 213(1–4): 291–321.

Sultan, N. Cochonat, P. Foucher, J.P. & Mienert, J. 2004b. Effect of gas hydrates melting on seafloor slope instability. *Marine Geology* 213(1): 379–401.

Waite, W.F. Santamarina, J.C. Cortes, D.D. Dugan, B. Espinoza, D.N. Germaine, J. Jang, J. Jung, J.W. Kneafsey, T.J. Shin, H. Soga, K. & Winters, W.J. 2009. Physical properties of hydrate-bearing sediments. *Reviews of Geophysics* 47(RG4003): 1–38.

Wu, L. Grozic, J.L.H. & Eng, P. 2008. Laboratory Analysis of Carbon Dioxide Hydrate-Bearing Sands. *Journal of Geotechnical and Geoenvironmental Engineering* 134(4): 547–550.

Zibib, H.M. & Aifantis, E.C. 1988. On the Localization and Postlocalization Behavior of Plastic Deformation.1. On the Initiation of Shear Bands. *Res Mechanica* 23: 261–277.